Electronic Supplementary Material (ESI) for Physical Chemistry Chemical Physics.

Supplementary Information for: **Role of Cationic Group in Defining Structural and Dynamic Correlations in Anion Exchange Membrane: A Molecular Dynamics Simulation Study of Hydrated Quaternary Ammonium-functionalized Poly(p-phenylene oxide)-based Membrane.**

Dengpan Dong, Xiaoyu Wei, Justin B. Hooper, Hongchao Pan, Dmitry Bedrov*

Department of Materials Science & Engineering, University of Utah, 122 South Central Campus Drive, Room 304, Salt Lake City, Utah 84112, United States

DFT calculations. The benchmark structure of hydroxide-water cluster is shown in Figure S1, where four water molecules were found within the same plane. At geometry predicted by quantum chemistry calculation, the force field of hydroxide was fitted in the way that the same binding energy -73.77 kcal/mol was reproduced.

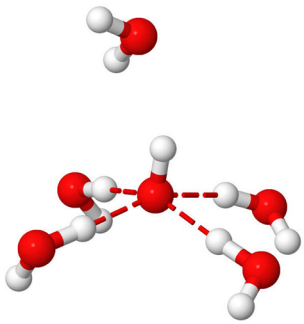

Figure S1. Benchmark structure for the parameterization of hydroxide force field. The optimization is performed utilizing quantum chemistry package Gaussian09 with theory M052X and aug-cc-pVDZ basis set. Hydrogen bond is shown in red dashed line.

Structural correlations. The N^+-N^+ correlation at hydration level λ=5 is illustrated in Figure S2 A. Featured correlation at 6 Å has been observed in $3R_1$ and asymmetrical functional groups, while no significant N^+-N^+ correlation was found in $3R_2$ and $3R_3$ systems. From comparison of relative contributions to the total correlation, shown in Figure S2 B, the inter-molecular contribution to N^+-N^+ correlation is the dominant one.

The hydration structure of polymer at λ=5 has been characterized by N^+-O_w correlation shown in Figure S2 A. The positions of the first maxima and first minima are located at around 4

Å and 6 Å, respectively. In the case of N^+-O_w correlation in $3R_2$, an extended shoulder has been observed in the first peak, which is consistent with the correlational feature at λ=10. The strength of this correlation, as indicated by the height of first correlation peak, decays with increasing alkyl group length on the functional group. Asymmetrically modified functional groups, however, show similar N^+-O_w correlation. Conclusively, N^+-O_w correlation is dominated by accessibility of central N^+ to water.

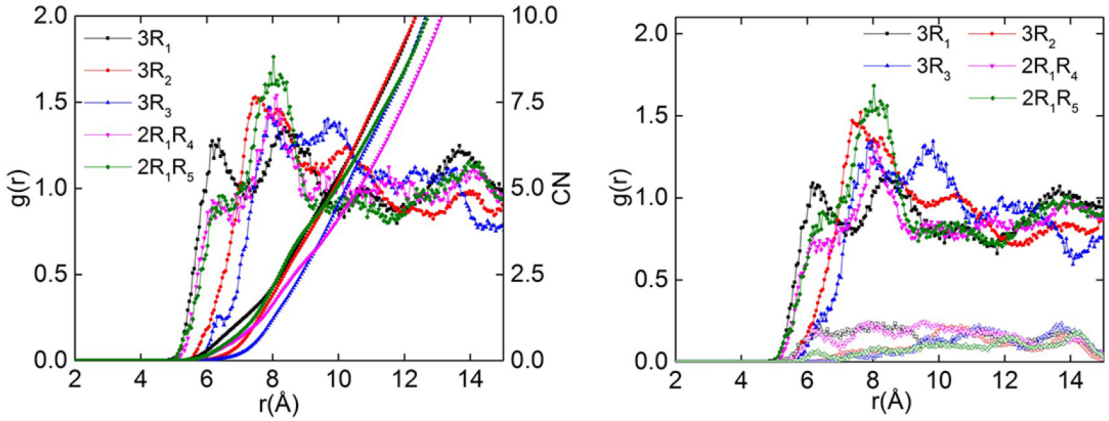

Figure S2. N^+-N^+ correlation at hydration level λ=5 (A), and corresponding inter- and intra-molecular contribution to total N^+-N^+ correlation (B).

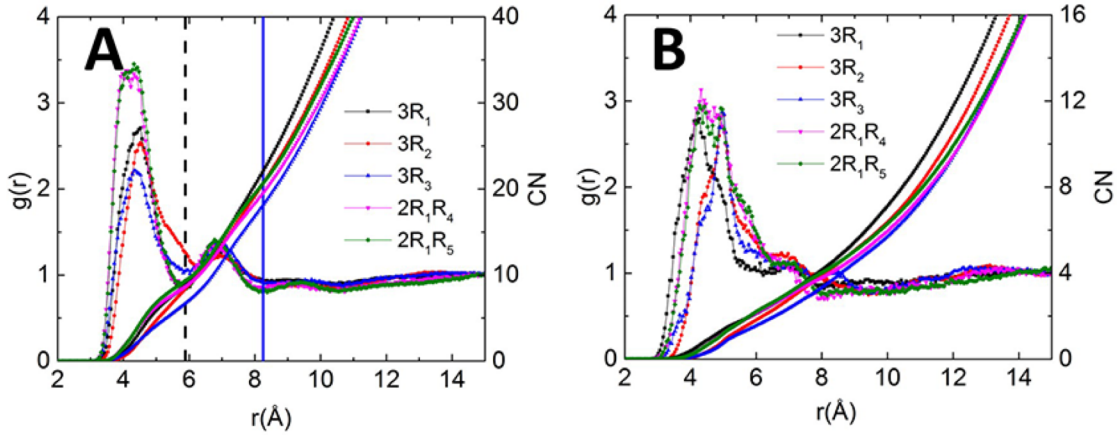

Figure S3. N^+-O_w correlation(A) and N^+-O^- correlation(B) at hydration level λ=5. Dashed black line defines the boundary between first and second hydration shell. The second hydration shell of cation is located between dashed black line and solid blue line.

The N^+-O^- correlation is illustrated in Figure S3 B, in which two significantly different correlation patterns can be identified. First, the N^+-O^- correlation peak in $3R_1$ and asymmetric

functional groups is located at around 4 Å, overlapping with the first N^+-O_w correlation peak. Scaled with increasing chain length, the location of the first N^+-O^- correlation peak in $3R_2$ and $3R_3$ shifts to larger separations, indicating an increased protection of the central N^+ from possible attacks by OH^-.

Water channels structure. The structure of the water channel in AEMs with asymmetrically modified functional groups is shown Figure S4. The hydration level shows the most significant impact on the morphology of these water channels, where the size of water domains increases dramatically with increasing hydration. At λ=10, minor difference can be observed between water channel in $2R_1R_4$ and $2R_1R_5$. However, the distribution of channel size illustrates the exact difference in the morphology of water channel. The distribution of water channel sizes is estimated by the following methodology to estimate pore-size-distribution (PSD). Several minor modifications to this protocol were made to adapt it to our systems. The PSD is usually estimated between significantly different phases. In PPO-based AEM systems, side chains of polymer can move slightly during simulation, where the water channel can be straightforwardly defined based on relative water density. Averaging of local water density (calculated on a regular grid) in our simulation was performed to map the structure of water channel. In our simulation, the water channel is defined if the local water density is larger than 25% of bulk water density. To increase the computational efficiency, the core points, potential points for the center of drawn spheres, were placed in the regions where the water density was larger than 50% of bulk water density. The detailed algorithm to estimate the distribution of channel sizes is given in the diagram shown in Figure S5.

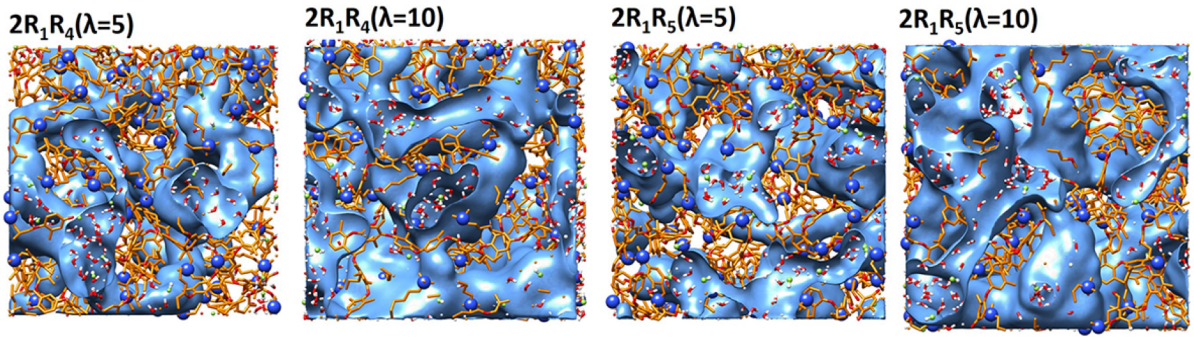

Figure S4. Structure of water-rich domain. The isosurface of water channel is drawn at 50% bulk water density.

The PSD at λ=10 is shown in Figure S6 A and B. Compared to $3R_1$, narrower channels were observed in the $3R_2$, while an opposite trend was seen in $3R_3$, *i.e.*, giving a broader size distribution. The averaged channel size decreases upon going from $3R_1$ to $3R_2$, while significantly higher probability for larger channel sizes is observed in PSD for $3R_3$. For polymer with asymmetric alkyl groups, the probabilities of large channel sizes are comparable to those in $3R_3$, while PSD at smaller sizes is noticeably reduced in $2R_1R_4$ and $2R_1R_5$.

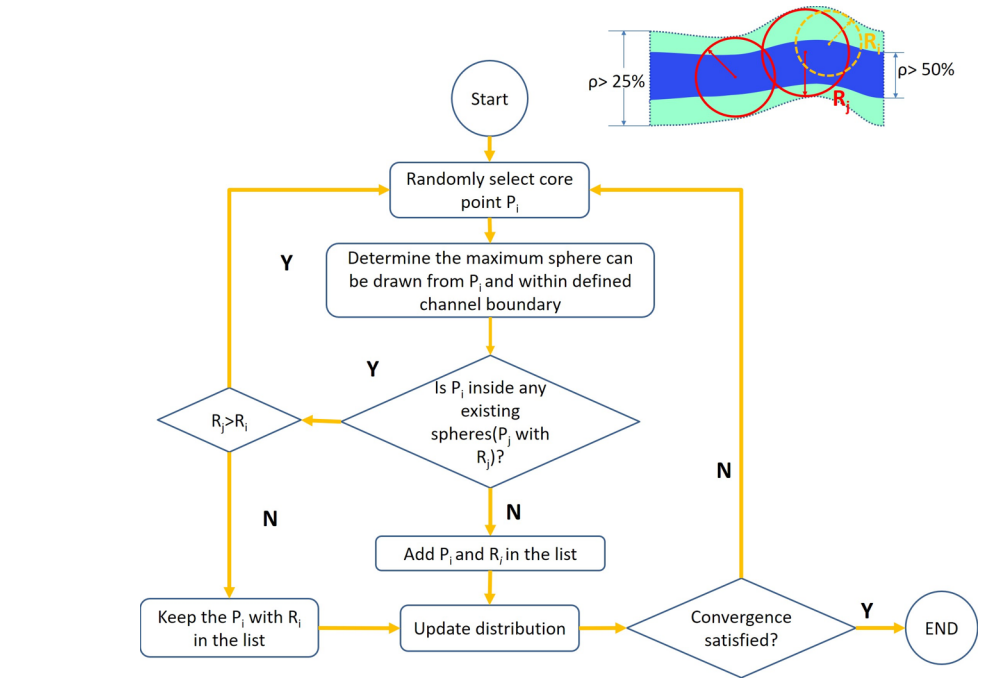

Figure S5. The algorithm to estimate distribution of water channel size. The top image shows the schematic illustration of this algorithm in a 2-D channel as an example.

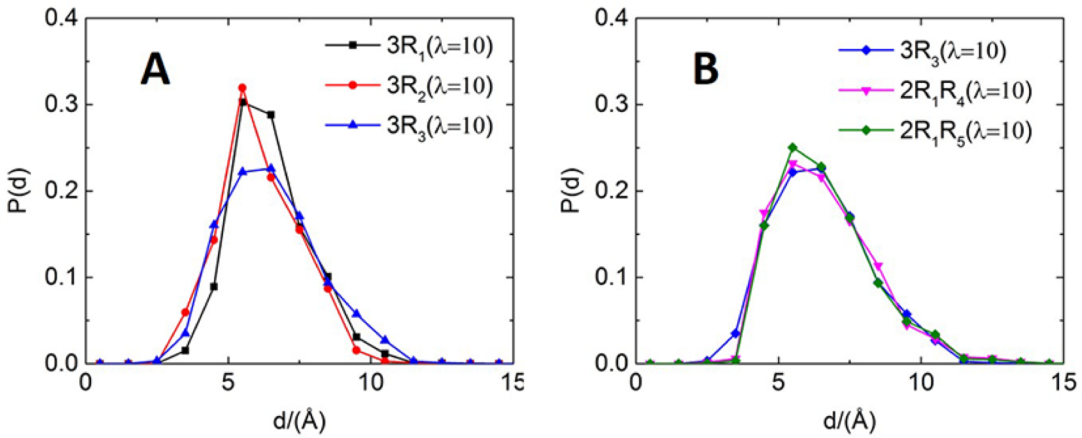

Figure S6. PSD for symmetrically (A) and asymmetrically (B) modified functional groups.

Dynamic heterogeneity. The non-Gaussianity parameter (α_2) is utilized to characterize heterogeneity in dynamics and is shown in Figure S7. The evolution of α_2 has been characterized both as a function of time (Figure S7 A and B) and as a function of MSD (Figure S7 C and D). If α_2 is close to zero, it means that displacements of OH^- follow Gaussian distribution. Typically, α_2 increases at glass transition or when experiencing structural heterogeneity. The overall non-Gaussianity behavior can be attributed to three origins: OH^--N^+ correlation, OH^--H_2O correlation and diffusion of OH^- between different water-rich domains in the water channel. The time scale corresponding to the appearance of heterogeneity decreases with increasing temperature. At 298 K, the first feature in dynamic heterogeneity is observed at 20 ps for both $3R_1$ and $2R_1R_4$, which is consistent with the residence time of water around OH^- within the first hydration shell. Considering the time scale, the non-Gaussianity behavior observed after 1 ns has two potential origins: N^+-O^- correlation and diffusion of OH^- through local water-rich domain. However, from Figure S7 C and D, the length scale for the appearance of the second feature in non-Gaussianity parameter is observed at MSD larger than 50 $Å^2$. The corresponding distance is significantly larger than the size of cation hydration shell or N^+-O^- correlation distance, as shown in N^+-O^- RDF.

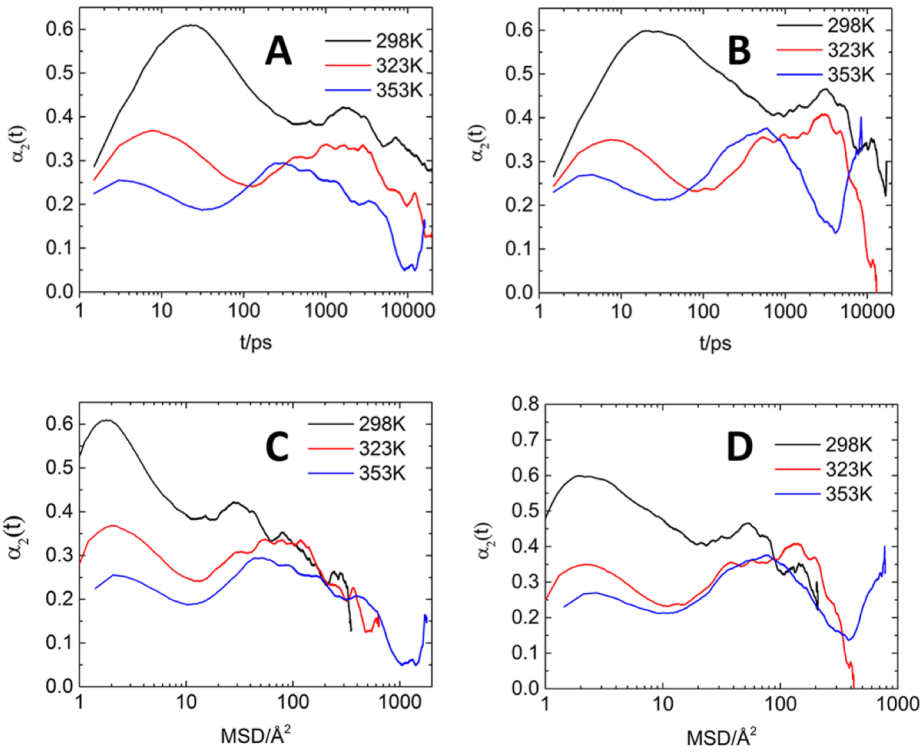

Figure S7. Non-Gaussianity parameter (α_2) of OH^- diffusion at hydration level λ=10; α_2 of $3R_1$ (A) and $2R_1R_4$ (B) with respect to time and α_2 of $3R_1$ (C) and $2R_1R_4$ (D) with respect to corresponding MSD.

The non-Gaussianity in membranes with asymmetric functional groups is shown in Figures S8 and S9. Compared to $2R_1R_5$, the timescale of featured heterogeneity in $2R_1R_4$ after 1 ns was significantly reduced. The second α_2 peak extends leftward to shorter times. This shift indicates that transport efficiency of OH^- is enhanced in $2R_1R_4$.

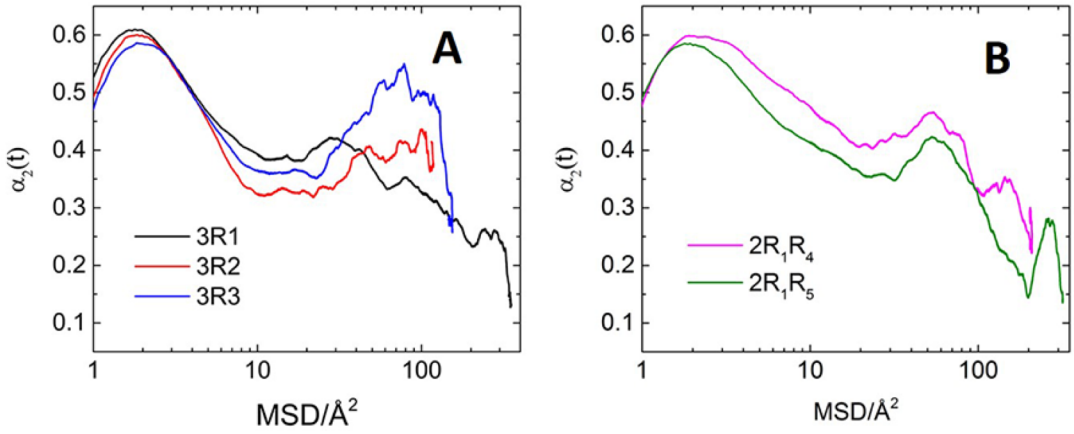

Figure S8. Non-Gaussianity parameter of symmetrically (A) and asymmetrically (B) modified functional groups at hydration level λ=10.

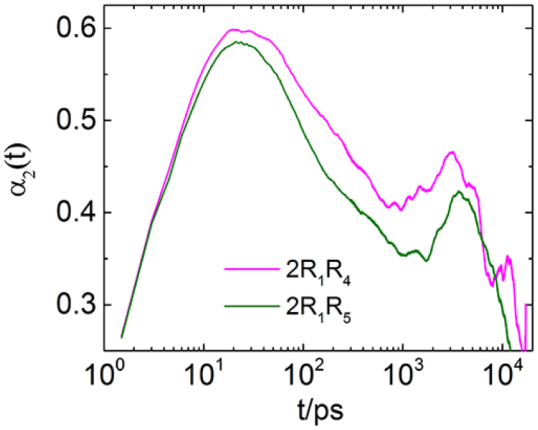

Figure S9. Non-Gaussianity parameter in polymers with asymmetric side chains.

Dynamic properties. Figure S10 shows the ratio of water diffusion coefficient and hydroxide as a function of hydration level. The ratio of D_{H2O}/D_{OH} in Figure S10 shows strong sensitivity to the structure of polymer/morphology of water channels at low hydration levels.

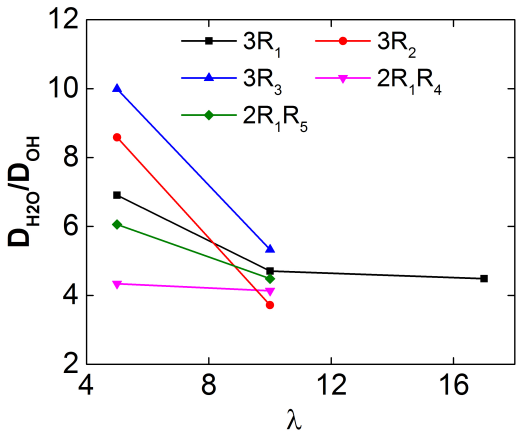

Figure S10. D_{H2O}/D_{OH} ratio at different hydration levels.

Figures S11 and S12 track the displacement and coordination number for a hydroxide or a water molecule diffusing through the same bottleneck. Figure S11 compares the results from simulations using non-reactive APPLE&P and reactive ReaxFF force fields. The latter explicitly includes the Grotthuss mechanism. The figure illustrates that if the Grothuss mechanism is present, the OH^- can transition through a bottleneck relatively fast and without any noticeable loss of its hydration shell, i.e. the OH- just hopes through the bottleneck by involving Grothuss mechanisms. In contrast, in the APPLE&P simulations where only the vehicular mechanism is available for OH^- transport, in order to pass through the bottleneck, it requires for OH^- to lose one or two water molecules from its hydration shell (e.g. see drop in the coordination number for t=0.5-0.8ns right before when OH- has sharp displacement increase). See refs. 38 for a more detailed discussion of these results.

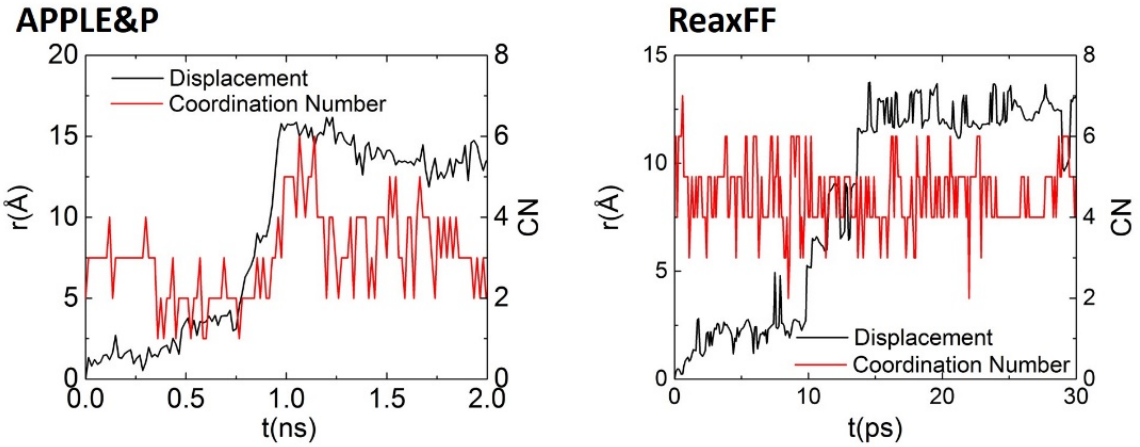

Figure S11. Displacement and coordination number evolution for OH^- diffusing through bottleneck: a comparison between reactive ReaxFF and non-reactive APPLE&P.

The transport of water molecules through bottlenecks occurs relatively smoothly without significant fluctuation in coordination number, allowing water molecule to pass through the bottleneck back and forth several times over 10ns time window.

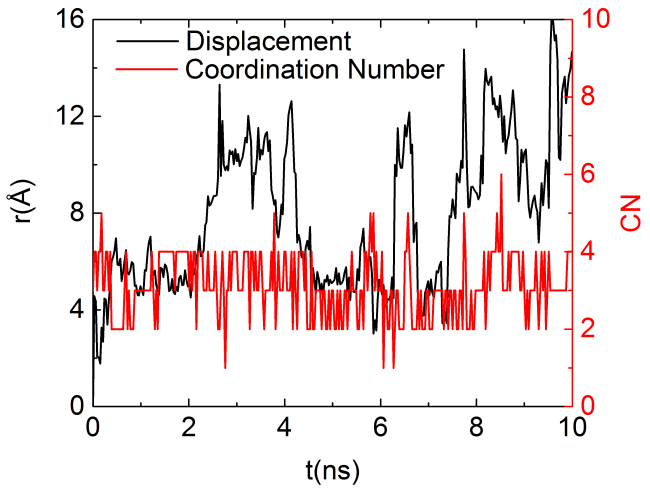

Figure S12. Displacement and coordination number evolution for a water molecule diffusing through the same bottleneck as in Figure S11.